Table of Contents

Methods and Materials

General

All chemicals, unless otherwise stated, were purchased from SigmaAldrich (St. Louis, MO) and were used as received. Water (>18.2 MΩ·cm at 25 ºC, Milli-Q, Millipore, Billerica, MA) was purified by passing through a 10 cm column of chelex resin (Bio-Rad Laboratories, Hercules, CA) at a flow rate <1.0 mL/min. All instruments were calibrated and maintained in accordance with previously reported routine quality-control procedures (*1*). Radioactivity measurements were made by using a Capintec CRC-15R Dose Calibrator (Capintec, Ramsey, NJ) with a calibration factor of 465 for ^{89}Zr. For accurate quantification of radioactivities, experimental samples were counted for 1 min. on a calibrated Perkin Elmer (Waltham, MA) Automatic Wizard^2 Gamma Counter by using a dynamic energy window of 800–1000 keV for ^{89}Zr (909 keV emission). ^{89}Zr-radiolabeling reactions were monitored by using silica-gel impregnated glass-fibre instant thin-layer chromatography (ITLC-SG) paper (Pall Corp., East Hills, NY) and analyzed on a radio-TLC plate reader (Bioscan System 200 Imaging Scanner) coupled to a Bioscan Autochanger 1000 (Bioscan Inc., Washington, DC, using Win-Scan Radio-TLC software version 2.2). Solvent systems included diethylene triamine pentaacetic acid in water (DTPA, 50 mM, pH7) and phosphate buffered saline (PBS). Human prostate cancer cell lines LNCaP and PC-3 were obtained from the American Type Culture Collection (ATCC, Manassas, VA) and were grown by serial passage.

Cell Lines

Human prostate cancer cell lines LNCaP and PC-3 were obtained from the American Type Culture Collection (ATCC, Manassas, VA). LNCaP cells were grown in RPMI-1640 medium, supplemented with 10% heat inactivated fetal calf serum (FCS, Omega Scientific, Tarzana, CA), 2 mM glutamine, 10 mM Hepes, 1 mM sodium pyruvate, 4.5 g/L glucose, 1.5 g/L sodium bicarbonate, and 100 units/mL of both penicillin and streptomycin. PC-3 cells were grown in F-12 Kaign's medium supplemented with 10% heat inactivated fetal calf serum (FCS, Omega Scientific, Tarzana, CA), 2mM glutamine, 1.5 g/L sodium bicarbonate, and 100 units/mL of both penicillin and streptomycin. Cell lines were maintained by weekly serial passage in a 5% CO_2(g) atmosphere at 37 ºC. Cells were harvested by using a formulation of 0.25% Trypsin and 0.53 mM EDTA in Hank's Buffered Salt Solution (HBSS) without calcium or magnesium.

Xenograft models

All animal experiments were conducted in compliance with Institutional Animal Care and Use Committee (IACUC) guidelines. Male athymic *nu*/*nu* mice (NCRNU-M, 20–22 g, 6–8 weeks old) were obtained from Taconic Farms Inc. (Hudson, NY), and were allowed to acclimatize at the MSKCC vivarium for 1 week prior to implanting tumors. Mice were provided with food and water *ad libitum*. LNCaP tumors were induced on the left shoulder by sub-cutaneous (s.c.) injection of 4.0×10^6 cells in a 200 μL cell suspension of a 1:1 v/v mixture of media with reconstituted basement membrane (BD Matrigel™, Collaborative Biomedical Products Inc., Bedford, MA). Similarly, PC-3 tumors were induced on the right shoulder by s.c. injection of 5.0×10^6 cells. Palpable LNCaP tumors (50–250 mm^3) developed after a period of 24–30 days. PC-3 tumors (70–90 mm^3) grew more rapidly with more uniform size distribution and were suitable for use for *in vivo* studies after 10–14 days. The tumor volume (V / mm^3) was estimated by external vernier caliper measurements of the longest axis, a / mm, and the axis perpendicular to the longest axis, b / mm. The tumors were assumed to be spheroidal and the volume was calculated in accordance with Equation 1 (*2*).

$$V = \frac{4\pi}{3}\cdot\left(\frac{a}{2}\right)^2\cdot\frac{b}{2} \qquad (1)$$

Acute biodistribution studies

Acute *in vivo* biodistribution studies were conducted to evaluate the uptake of ^{89}Zr-DFO-J591 in mice bearing s.c. LNCaP (50–250 mm^3) or PC-3 (70–90 mm^3) tumors. Mice were randomized before the study and were warmed gently with a heat lamp 5 min. before administering ^{89}Zr-DFO-J591 (0.55–0.74 MBq [15–20 μCi], 3–4 μg of mAb, in 200 μL 0.9% sterile saline for injection) *via* intravenous (i.v.) tail-vein injection (t=0 h). Animals (n=3–5, per group) were euthanized by CO_2(g) asphyxiation at 24, 48, 96 and 144 h post-injection and 12 organs (including the tumor) were removed, rinsed in water, dried in air for 5 min., weighed and counted on a gamma-counter for accumulation of ^{89}Zr-radioactivity. The mass of ^{89}Zr-DFO-J591 formulation injected into each animal was measured and used to determine the total number of counts (counts per minute, [c.p.m.]) by comparison to a standard syringe of known activity and mass. Count data were background- and decay-corrected and the percentage injected dose per gram (%ID/g) for each tissue sample was calculated by normalization to the total amount of activity injected.

Competitive inhibition studies were also performed *in vivo* to investigate the specificity of ^{89}Zr-DFO-J591 for PSMA. Non-radiolabeled J591 (5 mg/kg solution in 0.9% sterile saline, 0.3 mg/mouse) was added to the ^{89}Zr-DFO-J591 formulation to reduce the specific-activity (60-fold decrease: 3.04 MBq/mg [0.082 mCi/mg]) and biodistribution studies were performed at 48 h post-i.v. administration (n=4).

Small-animal immunoPET imaging

PET imaging experiments were conducted on a microPET Focus 120 scanner (Concorde Microsystems) (*3*). Mice were administered ^{89}Zr-DFO-J591 formulations (10.9–11.3 MBq [295–305 μCi], 60–62 μg of mAb, in 200 μL 0.9% sterile saline for injection) *via* i.v. tail-vein injection. Approximately 5 minutes prior to recording PET images, mice were anesthetized by inhalation of 1% isoflurane (Baxter Healthcare, Deerfield, IL)/oxygen gas mixture and placed on the scanner bed. PET images were recorded at various time-points between 3–144 h post-injection. List-mode data were acquired for between 10 and 30 min. using a γ-ray energy window of 350–750 keV, and a coincidence timing window of 6 ns. For all static images, scan time was adjusted to ensure a minimum of 20 million coincident events were recorded. Data were sorted into 2-dimensional histograms by Fourier re-binning, and transverse images were reconstructed by filtered back-projection (FBP) into a 128×128×63 (0.72×0.72×1.3 mm) matrix. The reconstructed spatial resolution for ^{89}Zr was 1.9 mm full-width half maximum (FWHM) at the center of the field-of-view (FOV). The image data were normalized to correct for non-uniformity of response of the PET, dead-time count losses, positron branching ratio, and physical decay to the time of injection but no attenuation, scatter, or partial-volume averaging correction was applied. An empirically determined system calibration factor (in units of [mCi/mL]/[cps/voxel]) for mice was used to convert voxel count rates to activity concentrations. The resulting image data were then normalized to the administered activity to parameterize images in terms of %ID/g. Manually drawn 2-dimensional regions-of-interest (ROIs) or 3-dimensional volumes-of-interest (VOIs) were used to determined the maximum and mean %ID/g (decay corrected to the time of injection) in various tissues (*4*). Images were analyzed by using ASIPro VM™ software (Concorde Microsystems).

Density Functional Theory (DFT) Calculations

All calculations were conducted using density functional theory (DFT) as implemented in the *Gaussian03* suite of *ab initio* quantum chemistry programs.(*5*) Geometry optimizations and vibrational frequency calculations were performed by using the restricted B3LYP exchange and correlation functionals. Hydrogen, carbon, nitrogen and oxygen atoms were described by using the all-electron, double-ζ 6-31+G(d) basis set.(*6-9*) The LANL2DZ basis set was used for both description of the valence electrons and the effective core potentials of the Zr atom. Normal self-consistent field (SCF) and geometry convergence criteria were employed and all structures were optimized in the gas phase without the use of symmetry constraints. Harmonic frequency analysis based on analytical second derivates was used to characterize the optimized geometries as local minima.

DFT Discussion

The complexation reaction between ^{89}Zr-chloride or ^{89}Zr-oxalate with the hexadentate, trihydroxamate chelate, desferrioxamine B (DFO) is shown in Figure 1A. In contrast to the more familiar coordination chemistry of radionuclides such as ^{64}Cu, ^{68}Ga, ^{111}In and $^{86/90}$Y, ^{89}Zr displays a number of distinct differences. In particular, the 4+ oxidation state imparts a strong preference for $^{89}Zr^{4+}$ ions to bind to highly electronegative (class a) hard donor atoms including oxygen, nitrogen and fluoride. Zirconium complexes have a high propensity towards hydrolysis in aqueous solution. In addition, the relatively large ionic radius of $^{89}Zr^{4+}$ allows the first coordination sphere to accommodate up to 8-donor atoms. In this respect, the ionic nature of most Zr^{4+} complexes and the higher coordination numbers means that the chemistry more closely resembles that of radio-lanthanides and radio-actinides such as ^{177}Lu and ^{225}Ac.

As a consequence of the complicated aqueous-phase chemistry, the nature of the most $^{89}Zr^{4+}$(aq.) species, including the ^{89}Zr-DFO complex is uncertain. Unfortunately, all attempts at crystallizing ^{89}Zr-DFO have been unsuccessful. Therefore, we conducted high level density functional theory (DFT) calculations to probe the structure, bonding and chemical/thermodynamic stability of ^{89}Zr-DFO with respect to expansion of the coordination sphere from 6- to 7- or 8-coordinate with the addition of one or two water molecules.

Supplemental Table 1. B3LYP optimised Cartesian coordinates of $[Zr(HDFO)]^{2+}$ (**1**).

Atom	*x*	*y*	*z*
40	0.338085	-0.52271	0.363192
7	-8.66646	-4.43015	-1.55362
6	-7.91488	-3.09817	-1.63175
6	-6.65244	-3.12451	-0.7742
6	-5.9079	-1.77714	-0.85865
6	-4.61901	-1.75133	-0.02035
6	-3.93588	-0.38115	-0.1317
7	-2.64158	-0.33321	0.545328
6	-2.24564	0.379886	1.594183
6	-3.18181	1.145649	2.493186
6	-2.86823	2.653829	2.513357
6	-3.0678	3.29499	1.135945
8	-3.66912	2.696323	0.238133
7	-2.54231	4.535697	0.984848
6	-2.58354	5.302695	-0.26391
6	-1.20212	5.421439	-0.93045
6	-0.61846	4.070221	-1.36605
6	0.833175	4.164258	-1.85774
6	1.464324	2.80491	-2.19718
7	1.432851	1.857637	-1.07261
6	2.248092	1.73771	-0.04007
6	3.455926	2.611709	0.166524
6	4.689447	1.788745	0.574522
6	5.001977	0.701805	-0.45847
8	4.223644	0.470926	-1.38854
7	6.151714	0.008119	-0.26344
6	6.593366	-1.08619	-1.13134
6	6.544437	-2.46291	-0.44749
6	5.155743	-2.93481	0.019554
6	4.165474	-3.24069	-1.11552
6	2.86244	-3.90287	-0.63934
7	2.009131	-3.00127	0.149191
6	1.847802	-2.87502	1.459418
6	2.454888	-3.79692	2.472055
8	-1.64345	-1.01416	-0.10723
8	-0.98831	0.385476	1.853897
8	0.394212	0.960584	-1.09123
8	1.956995	0.834172	0.833981
8	1.368857	-2.05075	-0.60255
8	1.109548	-1.89985	1.861174
1	-9.51935	-4.424	-2.12788
1	-8.08118	-5.20972	-1.87974
1	-8.94688	-4.64588	-0.58842
1	-8.62621	-2.3361	-1.30296
1	-7.69559	-2.94235	-2.6912
1	-6.91698	-3.33358	0.271943
1	-5.98798	-3.93217	-1.11199
1	-6.57923	-0.973	-0.52658
1	-5.66101	-1.56561	-1.90811
1	-3.92679	-2.52822	-0.36628
1	-4.84982	-1.96444	1.032172
1	-4.54994	0.42747	0.264402
1	-3.72832	-0.13484	-1.1785
1	-4.22401	0.982172	2.218307
1	-3.03452	0.74604	3.503907
1	-1.84527	2.818114	2.870419
1	-3.53913	3.137998	3.234322
1	-2.0686	4.953355	1.776981
1	-3.29232	4.793211	-0.92097
1	-2.98351	6.299313	-0.0456
1	-1.30088	6.091452	-1.79511

1	-0.50994	5.920431	-0.23539
1	-1.24827	3.632768	-2.15273
1	-0.66416	3.373404	-0.52058
1	0.893185	4.784743	-2.76221
1	1.448855	4.668383	-1.09923
1	2.503425	2.911259	-2.52033
1	0.919884	2.301387	-2.99911
1	3.666742	3.191966	-0.73347
1	3.224841	3.322526	0.970522
1	4.517404	1.315836	1.548602
1	5.545337	2.463885	0.693577
1	6.752649	0.276404	0.506736
1	5.95748	-1.05378	-2.01832
1	7.620046	-0.87901	-1.45466
1	6.966671	-3.19579	-1.14879
1	7.219811	-2.45157	0.419146
1	4.72845	-2.18004	0.694686
1	5.30028	-3.84321	0.621889
1	3.916492	-2.33263	-1.67546
1	4.625023	-3.94106	-1.82648
1	3.065836	-4.7877	-0.03147
1	2.250605	-4.21141	-1.49155
1	1.662931	-4.13328	3.148876
1	2.952245	-4.66458	2.039536
1	3.179527	-3.23625	3.073063

Supplemental Table 2. B3LYP optimised Cartesian coordinates of [Zr(HDFO)-*axial*-(H_2O)]$^{2+}$ (**2-ax**).

Atom	*x*	*y*	*z*
40	0.454322	-0.40634	1.077419
7	-8.3899	-4.54856	-1.76821
6	-7.48125	-3.33901	-2.00743
6	-6.41909	-3.22065	-0.91788
6	-5.52473	-1.98847	-1.15988
6	-4.43855	-1.81343	-0.08549
6	-3.62624	-0.53814	-0.35294
7	-2.52728	-0.34015	0.591907
6	-2.4106	0.543805	1.57474
6	-3.57345	1.331113	2.127799
6	-3.3908	2.854813	2.024543
6	-3.44924	3.339328	0.571716
8	-3.91686	2.622825	-0.31973
7	-2.96927	4.587609	0.353086
6	-2.83791	5.197964	-0.97304
6	-1.3763	5.248697	-1.45049
6	-0.73214	3.86205	-1.57126
6	0.758948	3.909798	-1.92979
6	1.43004	2.530515	-1.97911
7	1.415521	1.821003	-0.69016
6	2.337265	1.778958	0.252006
6	3.568302	2.645101	0.264517
6	4.857911	1.824731	0.431855
6	5.05724	0.848135	-0.73004
8	4.281711	0.832578	-1.68959
7	6.119622	0.008288	-0.61768
6	6.476992	-0.9857	-1.63062
6	6.369752	-2.43488	-1.12688
6	4.98268	-2.87015	-0.62116
6	3.869478	-2.80996	-1.6785
6	2.558452	-3.47646	-1.23639
7	1.918292	-2.79316	-0.10273
6	1.766173	-3.16397	1.153971
6	2.23827	-4.46587	1.726836
8	-1.40554	-1.07543	0.322255
8	-1.25057	0.661202	2.109108
8	0.334982	1.008867	-0.47852
8	2.124207	0.963458	1.231147
8	1.429767	-1.56048	-0.41303
8	1.165757	-2.31794	1.926656
1	-9.10844	-4.6392	-2.49804
1	-7.8519	-5.42434	-1.75492
1	-8.87567	-4.47845	-0.865
1	-8.14486	-2.47092	-2.03754
1	-7.0468	-3.48528	-2.9997
1	-6.90258	-3.13431	0.065539
1	-5.79936	-4.1282	-0.89985
1	-6.154	-1.0882	-1.1925
1	-5.0491	-2.07364	-2.14652
1	-3.76669	-2.68045	-0.07833
1	-4.90244	-1.752	0.908519
1	-4.24366	0.36199	-0.33721
1	-3.14993	-0.58381	-1.33754
1	-4.51075	1.039104	1.653389
1	-3.64136	1.061159	3.189326
1	-2.44905	3.155578	2.497575
1	-4.19848	3.339391	2.588085
1	-2.58559	5.095368	1.141169
1	-3.45092	4.602354	-1.65348
1	-3.2612	6.2078	-0.93389

1	-1.35521	5.767328	-2.41865
1	-0.79185	5.87243	-0.75709
1	-1.27088	3.270784	-2.32467
1	-0.85235	3.323537	-0.62467
1	0.898238	4.371156	-2.91722
1	1.296828	4.547973	-1.21407
1	2.470689	2.589908	-2.30374
1	0.909768	1.860984	-2.66916
1	3.623153	3.257729	-0.63605
1	3.473129	3.324896	1.121051
1	4.833862	1.275816	1.380514
1	5.710784	2.513221	0.483105
1	6.728522	0.109971	0.185549
1	5.815868	-0.80882	-2.48118
1	7.503084	-0.79452	-1.96712
1	6.683776	-3.09082	-1.95066
1	7.101222	-2.59078	-0.32174
1	4.701798	-2.25204	0.242738
1	5.075579	-3.90066	-0.2478
1	3.660758	-1.77406	-1.96565
1	4.19083	-3.33729	-2.58755
1	2.722343	-4.51803	-0.95181
1	1.824529	-3.45427	-2.04775
1	3.017513	-4.26712	2.471575
1	1.401643	-4.94282	2.247989
1	2.636328	-5.15715	0.98461
8	0.829257	-0.24821	3.404035
1	1.033455	-1.11509	3.797123
1	0.098621	0.157212	3.901728

Supplemental Table 3. B3LYP optimised Cartesian coordinates of [Zr(HDFO)-*equatorial*-$(H_2O)]^{2+}$ (**2-eq**).

Atom	*x*	*y*	*z*
40	0.39412	-0.77005	0.686356
7	-8.93805	-3.94024	-1.85971
6	-8.00708	-2.73087	-1.98328
6	-6.80403	-2.86207	-1.05239
6	-5.88178	-1.63283	-1.16963
6	-4.6552	-1.71674	-0.24498
6	-3.8055	-0.44293	-0.36311
7	-2.59003	-0.47736	0.451002
6	-2.31511	0.17435	1.576637
6	-3.36195	0.897532	2.389774
6	-3.12214	2.414398	2.494459
6	-3.3723	3.126894	1.161957
8	-4.04884	2.598768	0.272621
7	-2.81612	4.356649	1.03819
6	-2.8663	5.15628	-0.18858
6	-1.50214	5.224724	-0.89595
6	-0.95864	3.85109	-1.31428
6	0.480532	3.907445	-1.84426
6	1.119876	2.528543	-2.06617
7	1.147284	1.691934	-0.85526
6	1.985079	1.716847	0.161623
6	3.082528	2.737542	0.311868
6	4.460435	2.085812	0.52335
6	4.857148	1.216059	-0.6721
8	4.043804	0.959278	-1.56475
7	6.125242	0.732288	-0.66782
6	6.640283	-0.1716	-1.69887
6	6.911976	-1.59301	-1.1773
6	5.713316	-2.30769	-0.52935
6	4.557091	-2.64706	-1.48435
6	3.448819	-3.4913	-0.83272
7	2.601753	-2.73994	0.108663
6	2.709482	-2.57163	1.422391
6	3.733995	-3.2711	2.267394
8	-1.57043	-1.22135	-0.09168
8	-1.10719	0.135503	2.009995
8	0.207019	0.693439	-0.80024
8	1.824409	0.817481	1.072383
8	1.612713	-2.00573	-0.49692
8	1.872682	-1.7824	1.988109
1	-9.752	-3.86274	-2.48316
1	-8.45079	-4.81381	-2.09636
1	-9.29358	-4.04222	-0.90061
1	-8.6216	-1.85788	-1.74846
1	-7.71708	-2.68519	-3.03617
1	-7.14776	-2.96303	-0.01314
1	-6.23826	-3.77128	-1.30035
1	-6.45588	-0.72668	-0.93224
1	-5.54623	-1.52786	-2.21035
1	-4.04618	-2.59085	-0.50772
1	-4.98201	-1.8449	0.796243
1	-4.36322	0.455529	-0.09352
1	-3.45616	-0.30877	-1.39188
1	-4.36592	0.709627	2.007501
1	-3.29977	0.467375	3.396731
1	-2.1088	2.611287	2.862267
1	-3.8159	2.82264	3.240755
1	-2.26825	4.713982	1.811602
1	-3.61921	4.694491	-0.83125
1	-3.21216	6.164816	0.064408

1	-1.60737	5.879537	-1.77148
1	-0.77867	5.720102	-0.23064
1	-1.6172	3.405015	-2.07209
1	-0.99097	3.17658	-0.44991
1	0.517317	4.440819	-2.80365
1	1.103718	4.48838	-1.15026
1	2.146554	2.608009	-2.43368
1	0.552822	1.940971	-2.79127
1	3.111171	3.404003	-0.55133
1	2.84464	3.346064	1.193558
1	4.443194	1.465567	1.42771
1	5.205775	2.87274	0.690882
1	6.747665	1.008868	0.082021
1	5.899793	-0.1746	-2.50078
1	7.566212	0.250827	-2.10591
1	7.291473	-2.18852	-2.01891
1	7.7291	-1.55296	-0.4437
1	5.341402	-1.69114	0.300345
1	6.087859	-3.23834	-0.07938
1	4.109606	-1.73894	-1.90398
1	4.942201	-3.23507	-2.32887
1	3.867262	-4.35031	-0.30086
1	2.757601	-3.8708	-1.58934
1	4.410111	-2.52358	2.696308
1	3.223016	-3.75809	3.104546
1	4.326049	-4.00935	1.727698
8	-0.5691	-2.79417	1.699301
1	-1.26642	-3.15448	1.125931
1	-0.08949	-3.52576	2.119659

Supplemental Table 4. B3LYP optimised Cartesian coordinates of $[Zr(HDFO)\text{-}cis\text{-}(H_2O)_2]^{2+}$ (**3-*cis***).

Atom	*x*	*y*	*z*
40	0.492929	-0.33012	1.300166
7	-7.91224	-4.91793	-2.37052
6	-7.08604	-3.63172	-2.46397
6	-6.08225	-3.53469	-1.31823
6	-5.26458	-2.23196	-1.41722
6	-4.24778	-2.07226	-0.27449
6	-3.49877	-0.73913	-0.41233
7	-2.48391	-0.52549	0.618165
6	-2.47778	0.371278	1.596204
6	-3.7323	1.040131	2.108585
6	-3.70309	2.575104	2.044828
6	-3.83212	3.088905	0.607867
8	-4.2727	2.3661	-0.2926
7	-3.44909	4.37415	0.41045
6	-3.37902	5.009701	-0.90756
6	-1.94051	5.080215	-1.44879
6	-1.27316	3.704395	-1.56953
6	0.174028	3.766441	-2.07143
6	0.875073	2.402064	-2.09349
7	1.082213	1.809579	-0.76281
6	2.158808	1.844315	0.000186
6	3.313677	2.783832	-0.23618
6	4.668594	2.0601	-0.28429
6	4.723651	1.043244	-1.42568
8	3.71487	0.772618	-2.08395
7	5.924723	0.44674	-1.63845
6	6.124785	-0.61809	-2.62255
6	6.399698	-1.98906	-1.98109
6	5.341984	-2.48335	-0.97881
6	3.952514	-2.76611	-1.57272
6	2.979231	-3.42086	-0.57809
7	2.445127	-2.50288	0.442322
6	2.864542	-2.24712	1.670976
6	4.045173	-2.9206	2.308498
8	-1.31776	-1.22541	0.423795
8	-1.36262	0.591624	2.186998
8	0.107912	0.946557	-0.33587
8	2.167976	1.068339	1.024892
8	1.33315	-1.8129	0.03758
8	2.192978	-1.38765	2.349911
1	-8.59393	-4.99294	-3.1365
1	-7.31222	-5.75159	-2.40888
1	-8.43544	-4.96233	-1.48682
1	-7.80972	-2.81261	-2.45327
1	-6.60051	-3.66072	-3.4429
1	-6.61275	-3.56183	-0.35583
1	-5.40285	-4.39841	-1.34264
1	-5.95098	-1.37403	-1.41528
1	-4.73634	-2.20828	-2.38022
1	-3.5284	-2.90037	-0.28899
1	-4.76736	-2.10489	0.693229
1	-4.17463	0.1185	-0.39807
1	-2.95262	-0.70549	-1.36109
1	-4.61871	0.66955	1.592651
1	-3.81231	0.738333	3.160868
1	-2.79061	2.957715	2.516139
1	-4.54847	2.963295	2.627598
1	-3.06865	4.884471	1.198264
1	-4.0162	4.422161	-1.57267
1	-3.80793	6.014727	-0.83043

1	-1.97377	5.578052	-2.42776
1	-1.33787	5.72903	-0.79532
1	-1.8641	3.067718	-2.24258
1	-1.28812	3.20661	-0.59349
1	0.201538	4.162023	-3.09619
1	0.758773	4.465365	-1.45635
1	1.851886	2.451264	-2.57831
1	0.2814	1.662767	-2.63825
1	3.161656	3.366568	-1.14603
1	3.325907	3.48959	0.604278
1	4.844842	1.539941	0.665271
1	5.469045	2.802176	-0.39333
1	6.716291	0.7374	-1.07716
1	5.223112	-0.63889	-3.23757
1	6.962927	-0.34471	-3.27388
1	6.513427	-2.71878	-2.79466
1	7.371182	-1.95518	-1.46868
1	5.254055	-1.75008	-0.16554
1	5.728571	-3.40615	-0.52264
1	3.496176	-1.85092	-1.96647
1	4.053011	-3.46388	-2.41584
1	3.44894	-4.26569	-0.06577
1	2.093889	-3.79465	-1.09809
1	4.803992	-2.16528	2.540381
1	3.727767	-3.36207	3.259473
1	4.501394	-3.69248	1.689991
8	-0.4437	-2.11777	2.738521
1	-1.03582	-2.49131	2.055337
1	0.15225	-2.82289	3.038503
8	0.860447	0.56731	3.426785
1	1.590019	0.12525	3.895513
1	0.072672	0.579936	3.996493

Supplemental Table 5. Cartesian coordinates of B3LYP minimized geometry of [Zr(HDFO)-*trans*-$(H_2O)_2]^{2+}$ (**3-*trans***).[a]

Atom	*x*	*y*	*z*
40	0.560553	-0.27985	1.239486
7	-7.88444	-4.76074	-1.89651
6	-7.08956	-3.45598	-2.01529
6	-6.05997	-3.33349	-0.89624
6	-5.28015	-2.01025	-1.01983
6	-4.22493	-1.8286	0.082957
6	-3.51774	-0.47916	-0.09633
7	-2.41037	-0.27471	0.839764
6	-2.25924	0.625104	1.803564
6	-3.40158	1.407644	2.400051
6	-3.24322	2.931574	2.264853
6	-3.38998	3.392325	0.811204
8	-3.92717	2.671376	-0.0351
7	-2.90446	4.628713	0.534125
6	-2.89348	5.219337	-0.80661
6	-1.4955	5.203934	-1.44956
6	-0.91836	3.791544	-1.60665
6	0.504427	3.773172	-2.18155
6	1.135144	2.374265	-2.20885
7	1.267141	1.771661	-0.86835
6	2.23543	1.919895	0.008566
6	3.425977	2.817208	-0.19365
6	4.757001	2.062583	-0.0225
6	4.896699	0.914011	-1.02734
8	4.077942	0.76032	-1.93693
7	5.956588	0.08752	-0.82848
6	6.283127	-1.0423	-1.70121
6	6.242579	-2.39917	-0.97851
6	4.889302	-2.79712	-0.36285
6	3.761154	-3.00587	-1.38444
6	2.495444	-3.64321	-0.79331
7	1.882627	-2.82373	0.259424
6	1.609739	-3.13046	1.514871
6	1.908559	-4.48025	2.107952
8	-1.29077	-1.00816	0.552371
8	-1.07395	0.766309	2.279546
8	0.273194	0.90566	-0.50694
8	2.13154	1.238719	1.107987
8	1.543292	-1.55971	-0.12529
8	1.06879	-2.20449	2.22874
1	-8.5833	-4.85512	-2.64451
1	-7.26557	-5.57972	-1.9465
1	-8.38318	-4.81284	-0.99932
1	-7.83128	-2.65356	-1.98883
1	-6.62811	-3.47817	-3.0059
1	-6.56362	-3.37476	0.080145
1	-5.35797	-4.17815	-0.94023
1	-5.98915	-1.17097	-0.99126
1	-4.78365	-1.97055	-1.99852
1	-3.4826	-2.63381	0.029811
1	-4.69772	-1.87842	1.073701
1	-4.19654	0.369051	0.004497
1	-3.06811	-0.42243	-1.0931
1	-4.35592	1.096599	1.974347
1	-3.41089	1.151494	3.466885
1	-2.28265	3.251691	2.684316
1	-4.02719	3.41425	2.862558
1	-2.4654	5.149612	1.283525
1	-3.60223	4.644024	-1.4069
1	-3.26739	6.246675	-0.73552

1	-1.56986	5.698895	-2.42758
1	-0.8123	5.820069	-0.84548
1	-1.57987	3.190917	-2.2456
1	-0.91398	3.296495	-0.6286
1	0.504084	4.148909	-3.21376
1	1.15003	4.453936	-1.60849
1	2.126706	2.369567	-2.66687
1	0.505165	1.675517	-2.76403
1	3.388873	3.294699	-1.17312
1	3.374097	3.610859	0.562608
1	4.846988	1.678266	1.000261
1	5.581248	2.772559	-0.1668
1	6.607795	0.314716	-0.08643
1	5.575565	-1.00446	-2.53179
1	7.285451	-0.88617	-2.11808
1	6.559188	-3.16489	-1.70017
1	7.002997	-2.40264	-0.18498
1	4.585677	-2.0343	0.367124
1	5.04318	-3.72753	0.203139
1	3.490781	-2.05734	-1.8589
1	4.10069	-3.68128	-2.18181
1	2.716707	-4.61961	-0.35434
1	1.736483	-3.7799	-1.57197
1	1.568159	-4.48043	3.144704
1	1.387258	-5.27861	1.568848
1	2.980658	-4.703	2.089318
8	-1.24254	-1.08974	-2.63252
1	-0.73691	-0.76725	-1.86445
1	-0.60506	-1.16374	-3.35896
8	1.485962	0.121318	3.35888
1	2.190882	0.792456	3.373783
1	1.784494	-0.66202	3.852076

[a] As a result of dissociation of one of the water molecules from the axial coordination site, the complex failed to optimize under the normal convergence criteria. This failure to optimize was principally the result of large maximum and root-mean-square displacements arising from movement of the dissociated water molecule. Coordinates of the non-optimized but energy minimized structure are given in the table. This calculation was not included in the analysis and is presented only for completeness.

Supplemental Table 6. DFT calculated energetics and selected structural parameters for complexes **1**–**3**.

		Complex			
Parameter	**Donor Type**	**1**	**2-eq**[a]	**2-ax**[b]	**3-*cis***
Additional water molecules		2	1	1	0
Relative Energy / kJ mol^{-1}		0	-20	-61	-95
Bond lengths / Å					
r(Zr-O1)	C=O	2.176	2.215	2.209	2.26
r(Zr-O2)	N-O	2.081	2.100	2.122	2.12
r(Zr-O3)	C=O	2.164	2.171	2.165	2.19
r(Zr-O4)	N-O	2.078	2.094	2.107	2.11
r(Zr-O5)	C=O	2.192	2.197	2.261	2.25
r(Zr-O6)	N-O	2.095	2.161	2.116	2.20
r(Zr-OH_2(ax))	H_2O	-	-	2.362	2.33
r(Zr-OH_2(eq))	H_2O	-	2.460	-	2.47

[a] Equatorial = eq. [b] Axial = ax.

Supplemental Table 7. DFT calculated Mulliken and Natural Bond Order (NBO) atomic charges for selected atoms of complexes **1** – **3**.

		Complex			
Parameter	**Atom Type**	**1**	**2-eq**[a]	**2-ax**[b]	**3-*cis***
Mulliken Charges[c]					
Zr	-	2.739	2.956	2.481	2.945
O1	C=O	-0.606	-0.551	-0.791	-0.706
O2	N-O	-0.438	-0.456	-0.188	-0.355
O3	C=O	-0.573	-0.536	-0.646	-0.513
O4	N-O	-0.393	-0.319	-0.238	-0.267
O5	C=O	-0.526	-0.562	-0.609	-0.619
O6	N-O	-0.485	-0.468	-0.378	-0.367
N1	N-O	-0.218	-0.039	-0.35	-0.104
N2	N-O	-0.051	-0.081	-0.061	-0.106
N3	N-O	0.053	0.094	-0.096	0.054
N4	NH_3^+	0.53	0.53	0.529	0.528
O-ax	H_2O	-	-	0.071	0.023
O-eq	H_2O	-	0.209	-	0.267
NBO Charges					
Zr	-	2.458	2.431	2.371	2.329
O1	C=O	-0.0768	-0.757	-0.799	-0.777
O2	N-O	-0.675	-0.676	-0.652	-0.66
O3	C=O	-0.78	-0.765	-0.744	-0.759
O4	N-O	-0.674	-0.66	-0.66	-0.661
O5	C=O	-0.763	-0.764	-0.755	-0.77
O6	N-O	-0.685	-0.699	-0.666	-0.688
N1	N-O	-0.094	-0.103	-0.079	-0.096
N2	N-O	-0.093	-0.088	-0.08	-0.09
N3	N-O	-0.095	-0.096	0.091	-0.101
N4	NH_3^+	-0.806	-0.806	-0.806	-0.806
O-ax	H_2O	-	-	-0.976	-0.969
O-eq	H_2O	-	-0.981	-	-0.976

[a] Equatorial = eq. [b] Axial = ax. [c] Mulliken charges with summed hydrogens (i.e. atomic charges have been defined for heavy atoms only).

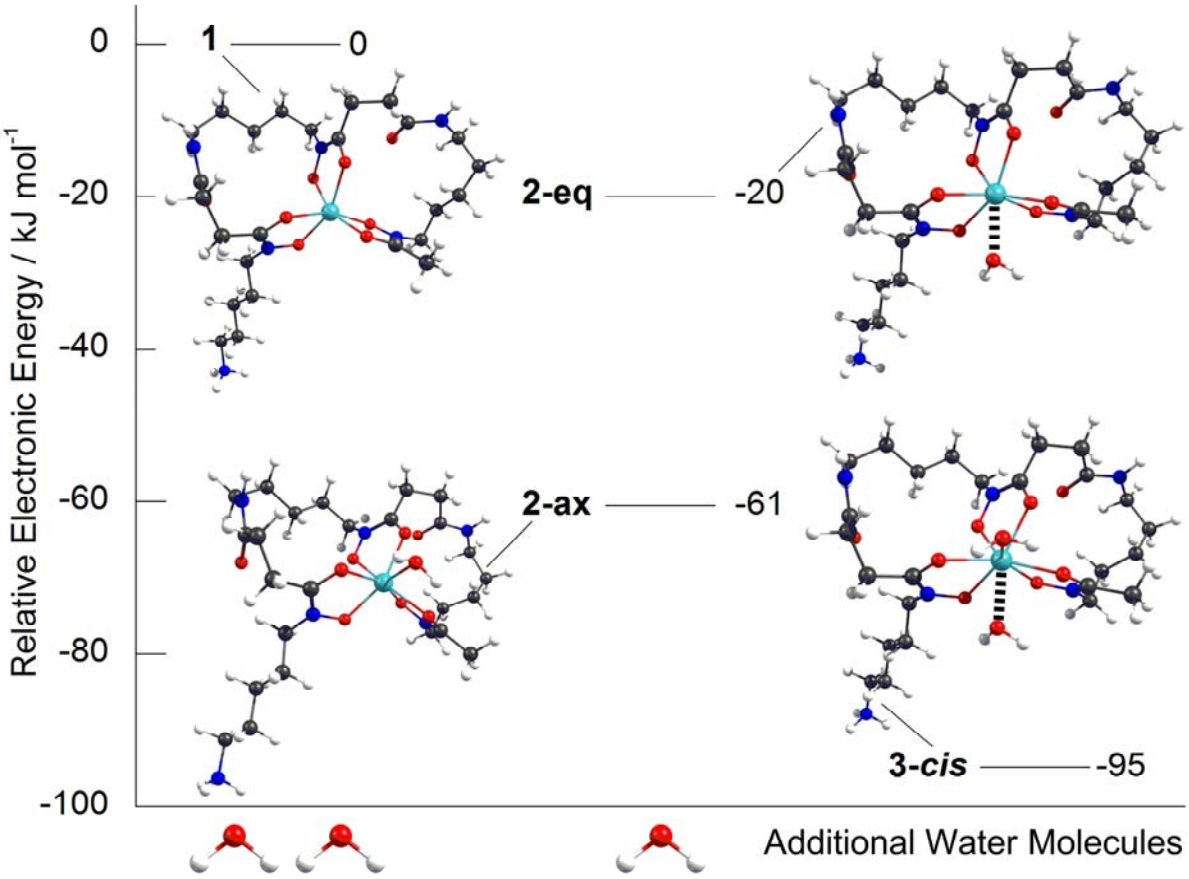

Supplemental Figure 1. DFT optimized reaction coordinate

DFT calculated reaction coordinate showing the relative calculated thermodynamic stability of the complexes formed by the addition of one or two water molecules to the hexa-coordinate complex, $[Zr(HDFO)]^{2+}$.

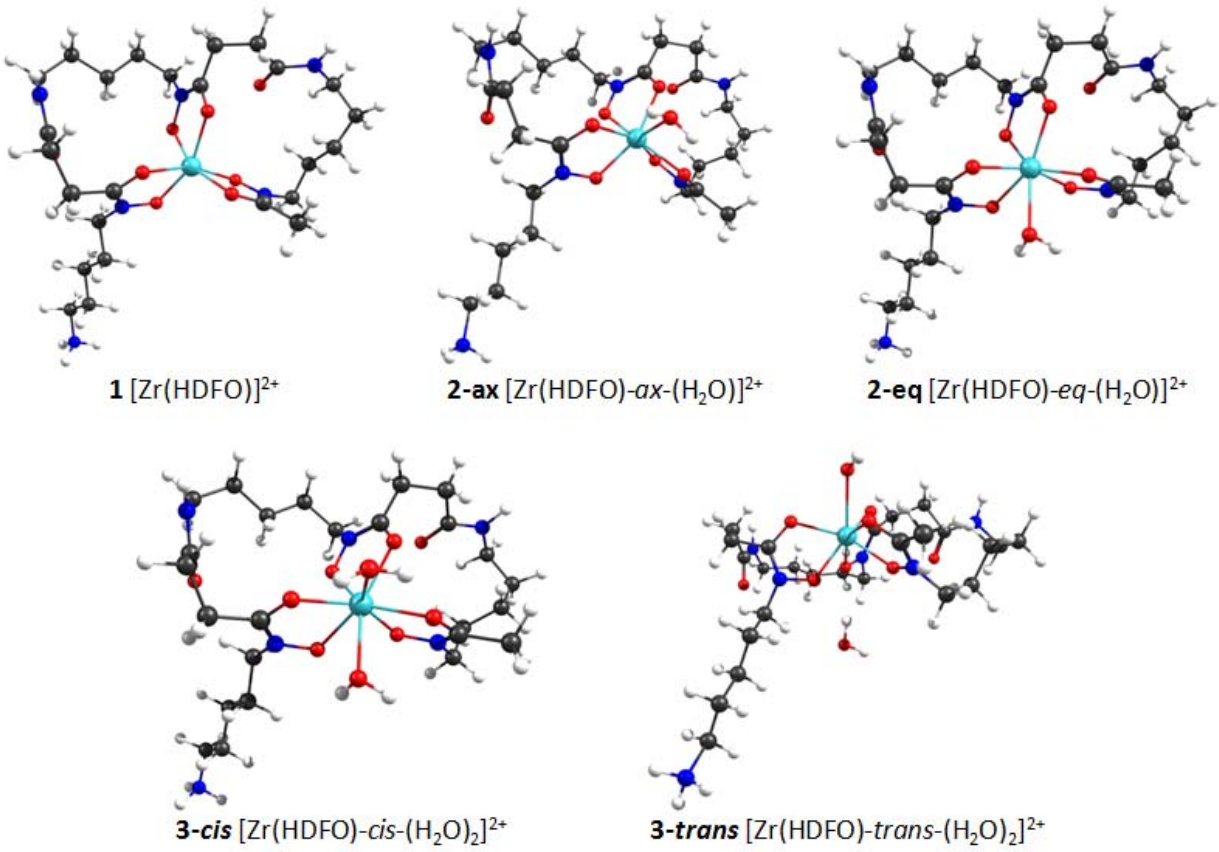

Supplemental Figure 2. DFT optimized structures of complexes 1 – 3

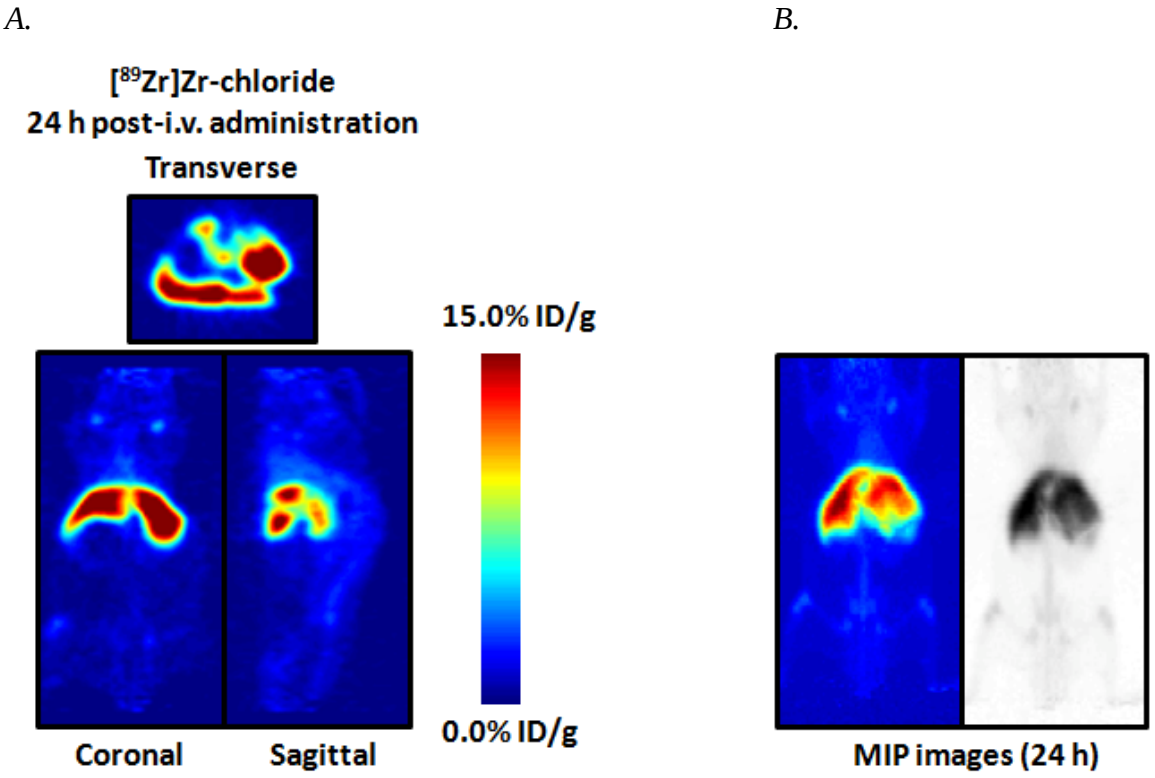

Supplemental Figure 3. PET imaging of ^{89}Zr-chloride

(A) Transverse, coronal and sagittal PET images of ^{89}Zr-chloride (300 μCi, 200 μL sterile saline) recorded at 24 h post-i.v. tail-vein administration in male, athymic, *nu*/*nu* mice. The images demonstrate that $^{89}Zr^{4+}$(aq.) ions (which are unstable with respect to hydrolysis) are sequestered in the liver. (B) Maximum intensity projection (MIP) images.

A. *B.*

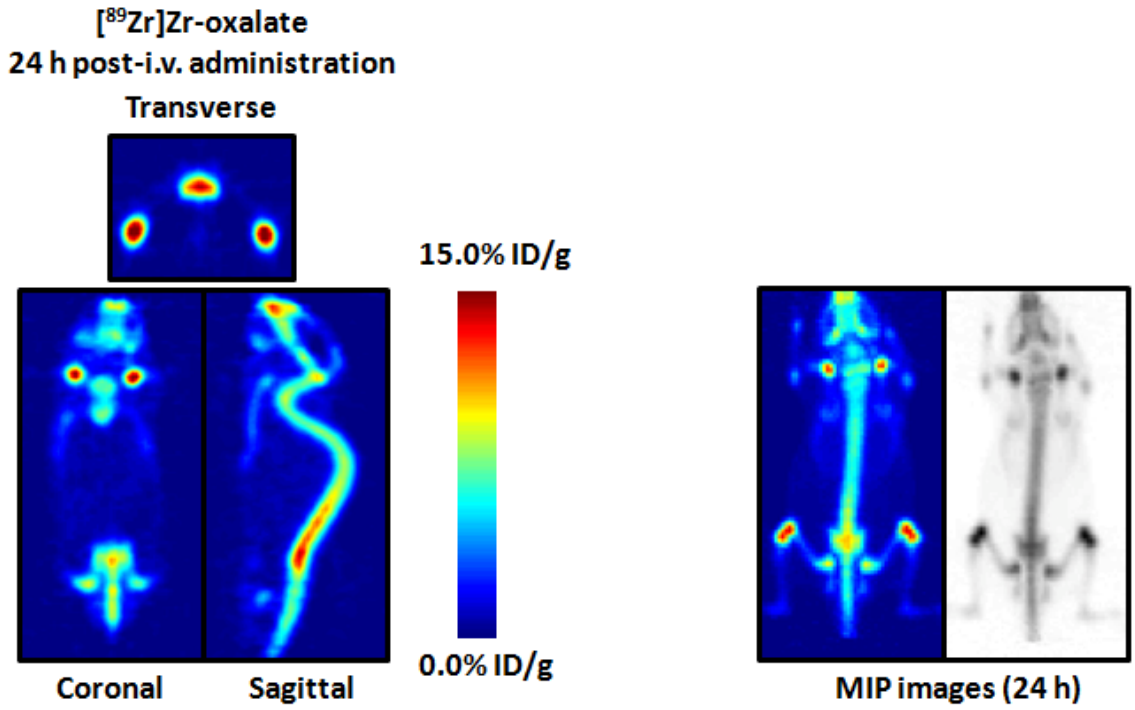

Supplemental Figure 4. PET imaging of ^{89}Zr-oxalate

(A) Transverse, coronal and sagittal PET images of ^{89}Zr-oxalate (300 μCi, 200 μL sterile saline) recorded at 24 h post-i.v. tail-vein administration in male, athymic, *nu*/*nu* mice. The images demonstrate that $[^{89}Zr(C_2O_4)_4]^{4-}$ complex ions are sequestered in the bone, bone marrow or cartilage. No uptake in thoracic or abdominal organs was observed. (B) Maximum intensity projection (MIP) images.

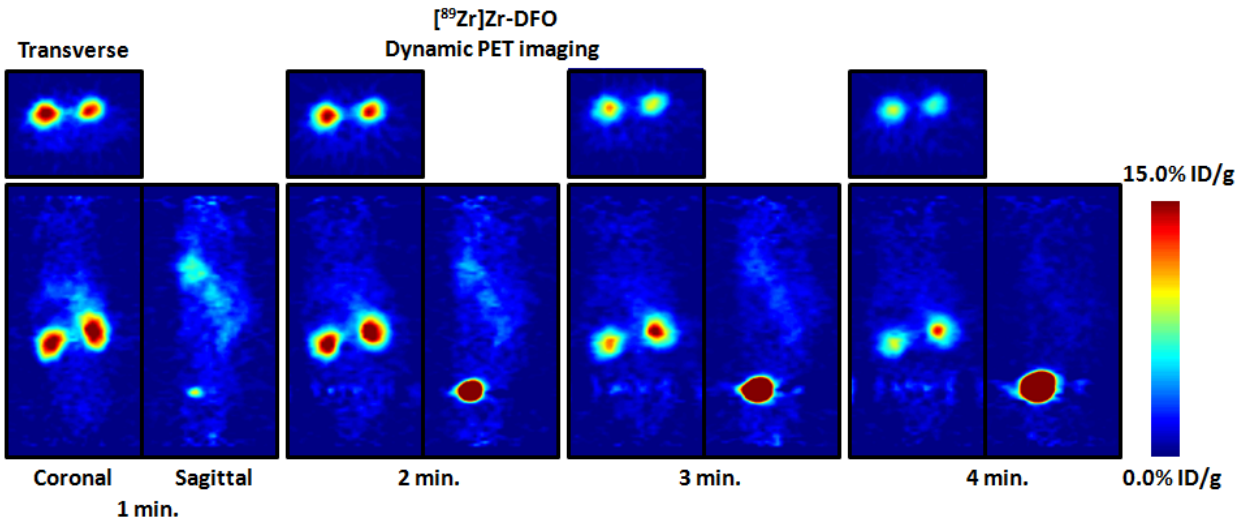

Supplemental Figure 5. Dynamic PET imaging of ^{89}Zr-DFO

Dynamic PET images of ^{89}Zr-DFO (300 μCi, 200 μL sterile saline) recorded at 24 h post-i.v. tail-vein administration in male, athymic, *nu*/*nu* mice. The transverse and coronal images lie in planes taken through the center of the kidneys. The sagittal images were taken through the main longitudinal (spinal) axis of the mouse passing through the center of the bladder. The same planes are presented for each frame (time point). The images demonstrate that hydrolytically stable ^{89}Zr-DFO is first-pass cleared by renal excretion. Within 0 – 2 min. post-injection high kidney uptake and excretion is observed, concurrent with accumulation of ^{89}Zr-radioactivity in the bladder. The kinetics of ^{89}Zr-DFO excretion is quantified in Supplemental Figures 6 (A) and (B).

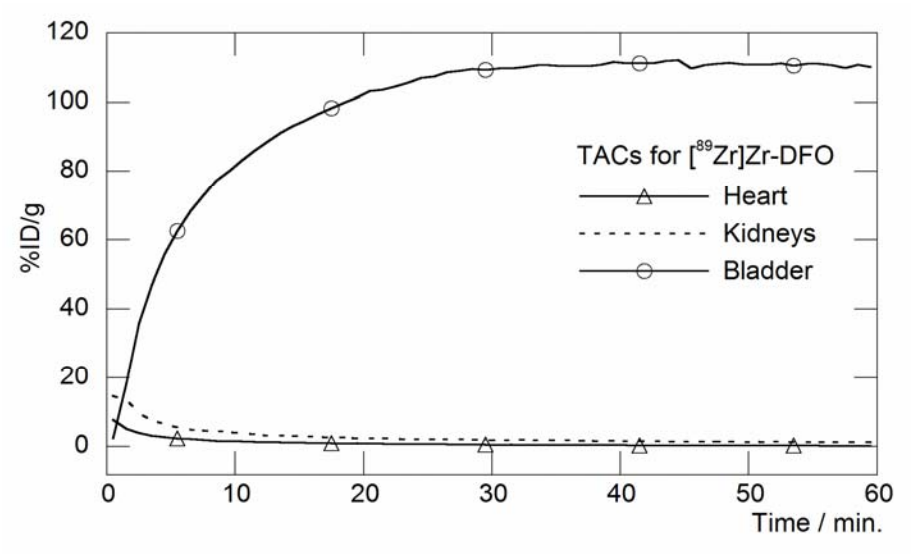

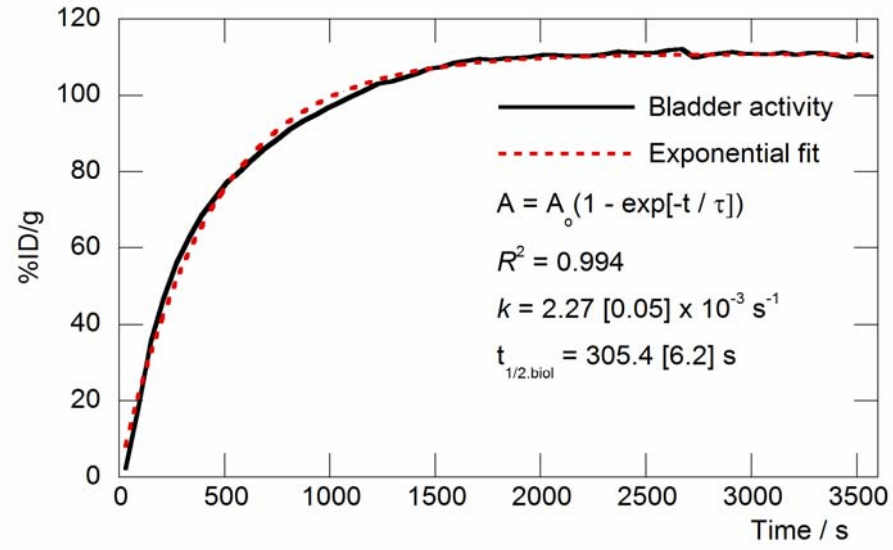

Supplemental Figure 6. Time-activity curves from ^{89}Zr-DFO PET imaging

A. Time-activity curves (TACs) of the heart, kidneys and bladder generated from volume of interest (VOI) analysis of the dynamic PET imaging study of ^{89}Zr-DFO in male, athymic, *nu*/*nu* mice.

B. Kinetic analysis of the renal excretions and accumulation of ^{89}Zr-radioactivity in the bladder post-i.v. administration of ^{89}Zr-DFO in male, athymic, *nu*/*nu* mice. Mathematical modeling of the data reveals that ^{89}Zr-DFO has a biological half-life, $t_{1/2.biol}$ = 305.4 ± 6.2 s, where k is the rate constant in s^{-1} ($k = 1/\tau$) and $t_{1/2.biol} = \ln 2/k$.

J591 conjugation

Synthesis of N-succinyldesferrioxamine B (N-succDFO) DFO mesylate (0.508 g, 0.77 mmol, Calbiochem, Spring Valley, CA) was dissolved in pyridine (7.5 mL) and reacted with excess succinic anhydride (1.704 g, 0.017 mol) at room temperature for 24 h. The white suspension was then poured into NaOH(aq.) (120 mL, 0.015 mol dm^{-3}) and stirred at room temperature for 16 h. The colorless solution was adjusted to pH2 by the addition of 12 mol dm^{-3} HCl and cooled with stirring at 4 ºC for 2 h. The white precipitate was collected by filtration, washed with copious amounts of HCl (0.01 mol dm^{-3}) then water and dried *in vacuo* to give the *N*-succinyldesferrioxamine B (*N*-succDFO) as a white microcrystalline solid (0.306 g, 4.75×10^{-4} mol, 62%). HRMS-ES^+: Calc. for $[C_{29}H_{52}N_6O_{11} + H^+]$ = 661.3772; found 661.3760 ($[M + H^+]$ = 100%).

Preparation of [Fe(N-succDFO-TFP)] activated ester *N*-succDFO (9.0 mg, 14 μmol) was suspended in 3.0 mL 0.9% sterile saline and the pH adjusted to 6.5 with 0.1 M Na_2CO_3(aq.) (50 – 75 μL in chelex purified water). Then a solution of $FeCl_3$•$6H_2O$ [4.0 mg, 15 μmol, 300 μL of 0.1 M HCl(aq.)] was added. Upon addition of the $FeCl_3$(aq.) the reaction mixture changes from colorless to deep orange due to the intense electronic absorption band of [Fe(DFO)] with a peak at 430 nm (ε_{430} = 2216 ± 49 mol^{-1} dm^3 cm^{-1}). After stirring the reaction at room temperature for 1 h, a solution of 2,3,5,6-tetrafluorophenol (TFP, 300 μL, 36 μmol, 1.2 mol dm^{-3} in chelex purified MeCN; SigmaAldrich, St. Louis, MO) was added to the reaction followed by addition of solid *N*-(3-dimethylaminopropyl)-*N'*-ethylcarbodiimide hydrochloride (EDAC, 120 mg, 0.63 mmol, SigmaAldrich) The reaction mixture (pH6.5) was then stirred at room temperature for 1 h before purifying the [Fe(*N*-succDFO-TFP)] product by use of a C-18 Light Sep-pak cartridge (Waters, Milford, MA). The reaction mixture was loaded onto a pre-activated (6 mL MeCN, 10 mL H_2O) C-18 cartridge, washed with copious amounts of water (>40 mL), and eluted with 1.5 mL MeCN. The final [Fe(*N*-succDFO-TFP)] solution had a concentration approximately 9.8 mM. The [Fe(*N*-succDFO-TFP)] solution can be stored for 24 h at 4 ºC but the most efficient conjugation reactions were achieved by using fresh preparations.

Preparation of DFO-J591 Humanized monoclonal antibody J591 (5 mg/mL, 1 mL, ~33 nmol, MW ~150,000 g mol^{-1}) was added to a centrifuge vial and the pH adjusted to 9.5 – 10.0 by using aliquots of 1.0 M and 0.1 M Na_2CO_3(aq.). Then 6 equivalents of [Fe(*N*-succDFO-TFP)] (200 nmol, 20 μL, 9.8 mM) was added and gently mixed using an automated pipette. The reaction was allowed to react at room temperature without agitation for 1 h. Then 2,5-dihydroxybenzoic acid [gentisic acid, 50 μL, 0.65 mol dm^{-3} in 0.32 M Na_2CO_3(aq.)] was added to the reaction and the pH was adjusted to 3.9 – 4.2 by the addition of 5 to 10 μL aliquots of 0.25 M H_2SO_4(aq.). Then a 10-fold excess of ethylenediaminetetraacetic acid disodium salt with [$EDTA^{2-}.2Na^{+}$(aq.), 0.0674 mol dm^{-3}, 13.7 μmol, 30 μL] with respect to [Fe(*N*-succDFO-TFP)] was added. The reaction was incubated in a water bath at 38 ºC for 1 h, during which time the solution changed from clear yellow to colorless. Subsequent purification led to colorless solutions which were found to have immunoreactive fractions >0.9. The DFO-J591 was purified by size-exclusion chromatography (Sephadex G-25 M, PD-10, >30 kDa, GE Healthcare; dead-volume = 2.5 mL, eluted with 200 μL fractions of 0.9% sterile saline).

Antibody radiolabeling

Zirconium-89 was produced *via* the $^{89}Y(p,n)^{89}Zr$ transmutation reaction on an EBCO TR19/9 variable beam energy cyclotron (Ebco Industries Inc., Richmond, British Columbia, Canada) in accordance with previously reported methods (*10, 11*). The ^{89}Zr-oxalate was isolated in high radionuclidic and radiochemical purity (RCP) >99.9%, with an effective specific-activity of 195–497 MBq/μg, (5.28–13.43 mCi/μg) (*10*).

^{89}Zr-DFO-J591 was prepared by the complexation of ^{89}Zr-oxalate with DFO-J591. Typical radiolabeling reactions were conducted in accordance with the following procedure. Briefly, ^{89}Zr-oxalate (153.2 MBq, [4.14 mCi]) in 1.0 M oxalic acid (170 μL) was adjusted to pH7.7–8.1 with 1.0 M Na_2CO_3(aq.). CAUTION: Acid neutralization releases CO_2(g) and care should be taken to ensure that no radioactivity escapes the microcentrifuge vial. After CO_2 evolution ceased, DFO-J591 (400 μL, 2.1 mg/mL [0.84 mg of mAb], in 0.9% sterile saline) was added and the reaction was mixed gently by aspirating with a pipette. The reaction was incubated at room temperature for between 1–2 h and complexation progress was monitored with respect to time by ITLC (DTPA, 50 mM, pH7). After 1 h, crude radiolabeling yields and RCP was >95%.

^{89}Zr-DFO-J591 was purified by using either size-exclusion chromatography (Sephadex G-25 M, PD-10 column, >30 kDa, GE Healthcare; dead-volume = 2.5 mL, eluted with 200 μL fractions of 0.9% sterile saline) or spin-column centrifugation (4 mL total volume, >30 kDa, Amicon Ultra-4, Millipore, Billerica, MA; washed with 4×3 mL, 0.9% sterile saline). The radiochemical purity (RCP) of the final ^{89}Zr-DFO-J591 (>77% radiochemical yield; formulation: pH5.5–6.0; <500 μL; 0.9% sterile saline) was measured by both radio-ITLC and analytical size-exclusion chromatography (loading <0.74 MBq [20 μCi], ca. 5–10 μL aliquots) and was found to be >99% in all preparations. In the ITLC experiment ^{89}Zr-DFO-J591 and ^{89}Zr-DFO remain at the baseline (R_f = 0.0), whereas $^{89}Zr^{4+}$(aq.) ions and ^{89}Zr-DTPA elute with the solvent front (R_f = 1.0).

Supplemental Figure 7 shows typical radio-ITLC chromatograms of the crude and purified ^{89}Zr-DFO-J591 and Supplemental Figure 8 shows a typical elution profile for the purification of ^{89}Zr-DFO-J591 by using PD-10 size-exclusion chromatography.

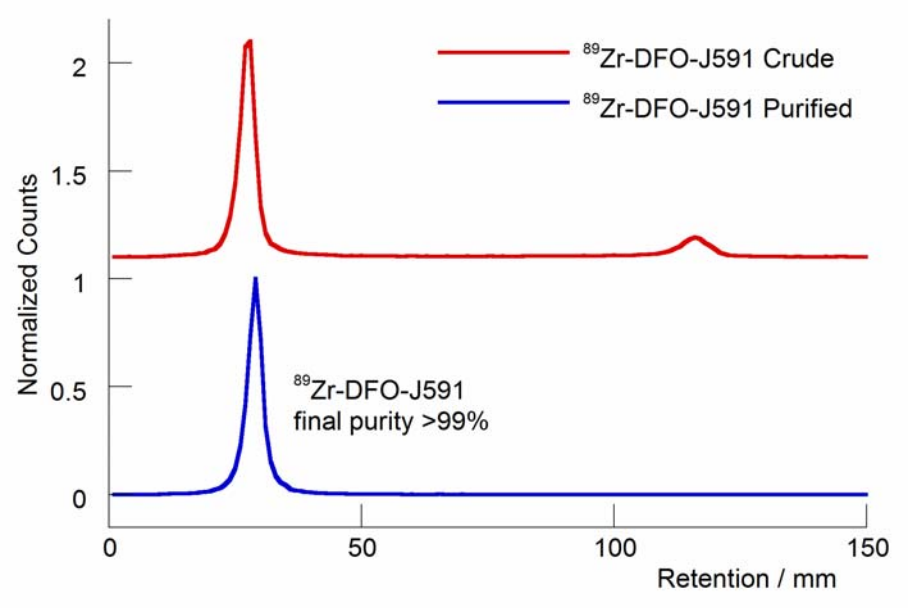

Supplemental Figure 7. Radio-ITLC

Typical radio-ITLC chromatograms of the crude (red) and purified (blue) ^{89}Zr-DFO-J591. Eluant: DTPA(aq.), 50 mM, pH7. The ^{89}Zr-DFO-J591 remains at the baseline (R_f = 0.0) and impurities run with the solvent front (R_f = 1.0).

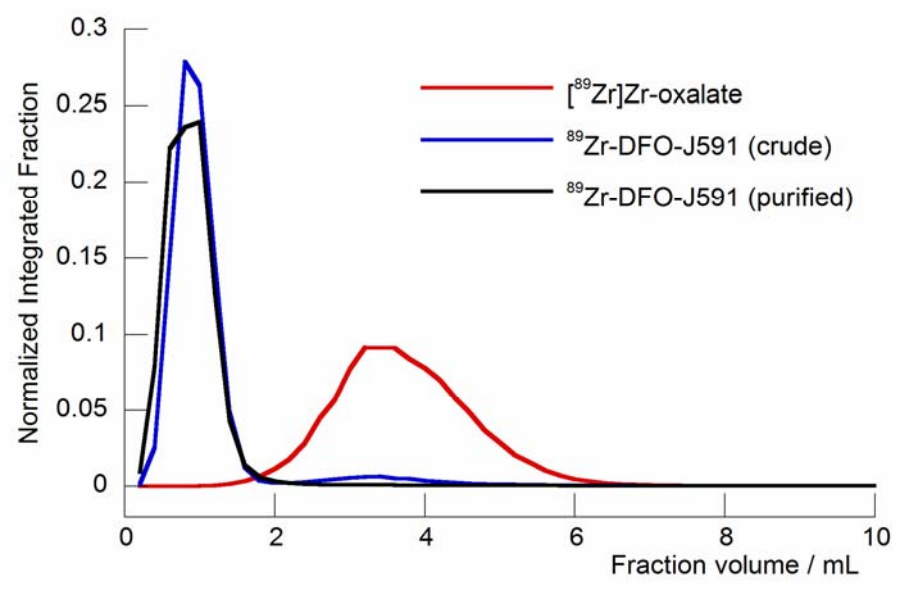

Supplemental Figure 8. Size-exclusion chromatography

Typical elution profiles observed by using PD-10 size-exclusion chromatography for the purification of ^{89}Zr-DFO-J591 from small molecule (<30 kDa) ^{89}Zr-radiolabeled impurities and unreacted ^{89}Zr-oxalate (complexed as ^{89}Zr-DTPA). Species with molecular weights >30 kDa elute in the first 1.8 mL of solvent. NB: the first 2.5 mL dead volume was discarded prior to collecting the fractions.

Chelate number

The number of accessible DFO chelates conjugated to J591 was measured by radiometric isotopic dilution assays following a method similar to that described by Anderson *et al*. (*12*) From a stock solution, aliquots of ^{89}Zr-oxalate (10 μL, 660 kBq [18 μCi], pH7.7–8.1 [pH adjusted using 1.0 M Na_2CO_3]) were added to 10 solutions containing 1:2 serial dilutions of non-radioactive $ZrCl_4$(aq.) (50 μL fractions; 250–0.5 pmol, pH7.7–8.1). The mixture was vortexed for 30 s before adding aliquots of DFO-J591 (5 μL, 2.1 mg/mL, [10.5 μg of mAb, 0.07 nmol], in 0.9% saline). The reactions were incubated at room temperature for 2 h before quenching with DTPA (20 μL, 50 mM, pH7). Control experiments confirmed that ^{89}Zr complexation to DFO-J591 was complete within <2 h. The extent of complexation was assessed by developing ITLC strips (DTPA, 50 mM) and counting the activity at the baseline and solvent front. The fraction of ^{89}Zr-radiolabeled mAb (A_b) was plotted *versus* the amount of non-radioactive $ZrCl_4$ added. The number of chelates was calculated by using linear regression analysis to calculate the concentration of $ZrCl_4$ at which only 50% of the DFO-J591 was labeled, multiplying by a factor of 2, and then dividing by the moles of mAb present in the reaction.

Immunoreactivity

The immunoreactive fraction of ^{89}Zr-DFO-J591 was determined by using specific radioactive cellular-binding assays following modified procedures derived from Lindmo *et al*. (*13*) Briefly, LNCaP or PC-3 cells were suspended in micro-centrifuge tubes at concentrations of 5.0, 4.0, 3.0, 2.5, 2.0, 1.5, and 0.5 $\times 10^6$ cells/mL in 500 μL PBS (pH7.4). Aliquots (50 μL, <0.37 kBq, [<0.01 μCi]) of ^{89}Zr-DFO-J591 in 1% bovine serum albumin (BSA) were added to each tube (n = 3; final volume: 550 μL) and the samples were incubated on an orbital mixer for 60 min. at room temperature. Cells were then pelleted by centrifugation (600G for 2 min.), resuspended and washed twice with ice-cold PBS before removing the supernatant and counting the ^{89}Zr-radioactivity associated with the cell pellet. The count data were background corrected and compared with the total number of counts in control samples. Non-specific binding was assessed by using the same methods but with PC-3 (PSMA-negative) cells in place of LNCaP cells. Immunoreactive fractions were determined by linear regression analysis of a plot of (total/bound) activity *versus* (1/[normalized number of cells]), and calculated as 1/y-intercept.

Supplemental Figure 9 demonstrates that the ^{89}Zr-DFO-J591 formulations are specific for expression of the PSMA antigen and have high immunoreactive fractions (0.95 ± 0.03). No weighting was applied to the data points. Data points are the mean of triplicate samples. Supplemental Figure 10 shows that after 7 days incubation in 1% bovine serum albumin solution at 37 ºC, ^{89}Zr-DFO-J591 remains active with an immunoreactive fraction of 0.78 ± 0.03.

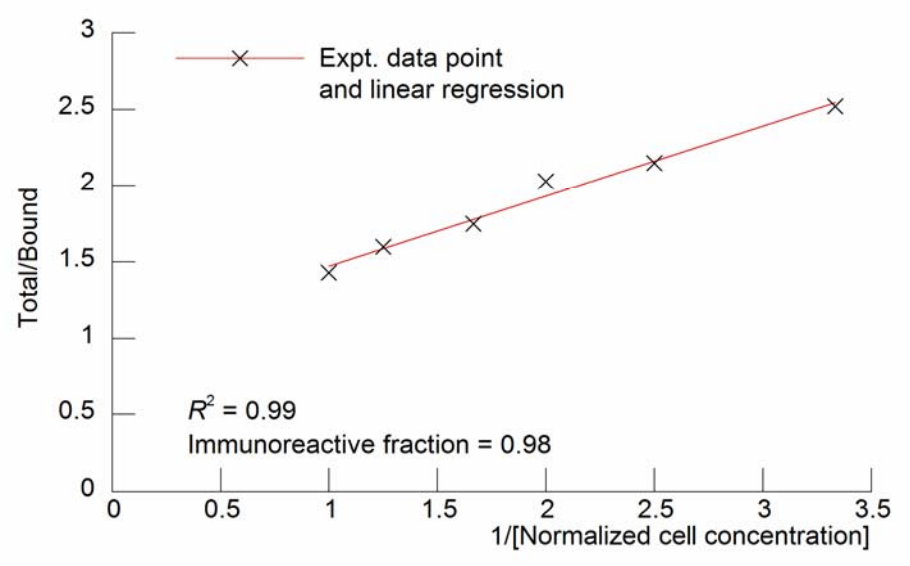

Supplemental Figure 9. Immunoreactivity of ^{89}Zr-DFO-J591 – day 1

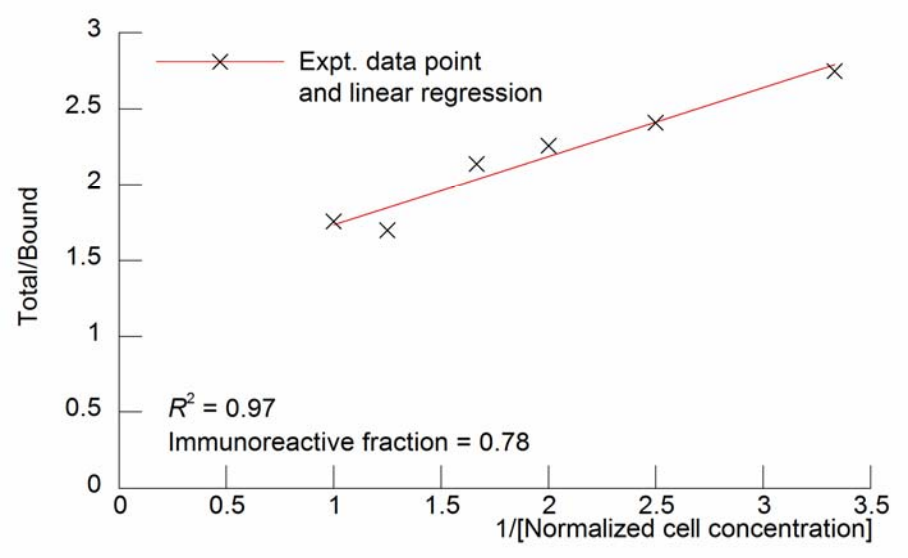

Supplemental Figure 10. Immunoreactivity of ^{89}Zr-DFO-J591 – day 7

Supplemental Table 8. Complete Biodistribution Data

Biodistribution data of ^{89}Zr-DFO-J591 *versus* time / h, administered by i.v. tail-vein injection to male, athymic *nu*/*nu* mice bearing either s.c. LNCaP (PSMA positive, 50–250 mm^3) or PC-3 (PSMA negative, 70–90 mm^3) tumors.[a,b]

	LNCaP (3 – 4 μg mAb)			
Organ	24 h (*n* = 4)	48 h (*n* = 5)	96 h (*n* = 5)	144 h (*n* = 4)
Blood	21.8 ± 2.8	4.4 ± 1.9	1.4 ± 0.8	2.6 ± 1.5
Tumor	34.4 ± 3.2	38.0 ± 6.2	40.4 ± 4.8	45.8 ± 3.2
Heart	7.4 ± 2.2	4.0 ± 1.3	1.7 ± 0.6	1.4 ± 0.5
Lung	11.7 ± 1.9	5.7 ± 3.1	2.2 ± 0.9	2.5 ± 0.9
Liver	11.7 ± 1.5	17.7 ± 1.6	17.2 ± 2.7	11.2 ± 1.6
Spleen	8.8 ± 4.3	21.1 ± 0.3	24.6 ± 1.8	4.6 ± 2.4
Stomach	1.1 ± 0.3	1.2 ± 0.2	1.1 ± 0.8	0.4 ± 0.1
Small Int.	1.6 ± 0.2	1.8 ± 0.3	1.2 ± 0.7	0.8 ± 0.1
Large Int.	3.8 ± 1.0	4.0 ± 1.9	4.4 ± 0.8	1.3 ± 0.5
Kidney	10.1 ± 1.0	7.5 ± 1.5	5.1 ± 0.5	5.3 ± 0.5
Muscle	1.1 ± 0.1	0.6 ± 0.3	0.4 ± 0.4	0.2 ± 0.2
Bone	4.0 ± 0.8	8.2 ± 1.2	8.7 ± 1.5	7.4 ± 1.3
Tumor/Blood	1.6 ± 0.2	8.7 ± 4.1	29.7 ± 17.1	18.0 ± 10.5
Tumor/Heart	4.7 ± 1.5	9.6 ± 3.5	23.4 ± 9.0	31.9 ± 10.7
Tumor/Lung	2.9 ± 0.5	6.7 ± 3.7	18.4 ± 7.7	18.5 ± 6.8
Tumor/Liver	2.9 ± 0.5	2.1 ± 0.4	2.3 ± 0.5	4.1 ± 0.7
Tumor/Spleen	3.9 ± 1.9	1.8 ± 0.3	1.6 ± 0.2	9.9 ± 5.2
Tumor/Stomach	31.7 ± 10.2	32.5 ± 7.4	36.4 ± 25.0	120.7 ± 40.5
Tumor/Sm. Int.	21.5 ± 3.5	21.1 ± 5.1	34.2 ± 19.1	59.5 ± 8.0
Tumor/Large Int.	9.1 ± 2.5	9.6 ± 4.8	9.3 ± 2.1	34.6 ± 12.5
Tumor/Kidney	3.4 ± 0.5	5.1 ± 1.3	7.9 ± 1.2	8.6 ± 1.1
Tumor/Muscle	32.4 ± 4.6	59.2 ± 28.8	95.9 ± 95.3	306.4 ± 432.2
Tumor/Bone	8.7 ± 1.9	4.7 ± 1.0	4.6 ± 1.0	6.2 ± 1.2

[a] The data are expressed as the mean %ID/g ± one standard deviation (S.D.). [b] Errors for the Tumor-to-tissue ratios are calculated as the geometric mean of the standard deviations.

Supplemental Table 8. Continued

	PC-3 (3 – 4 μg mAb)		**Block** (300 μg mAb)
Organ	48 h (*n* = 4)	96 h (*n* = 3)	48 h (*n* = 4)
Blood	19.0 ± 1.1	13.0 ± 1.8	10.7 ± 0.4
Tumor	15.6 ± 2.1	24.0 ± 2.6	10.3 ± 0.8
Heart	6.8 ± 0.1	4.3 ± 0.9	3.8 ± 0.7
Lung	12.6 ± 1.9	7.0 ± 2.3	5.7 ± 0.3
Liver	12.4 ± 0.9	11.0 ± 1.6	5.1 ± 0.4
Spleen	10.2 ± 2.0	7.2 ± 0.7	3.1 ± 0.7
Stomach	2.2 ± 0.8	1.9 ± 0.4	0.5 ± 0.2
Small Int.	1.4 ± 0.2	1.2 ± 0.2	0.9 ± 0.1
Large Int.	2.9 ± 0.4	2.7 ± 1.2	1.1 ± 0.1
Kidney	10.5 ± 0.9	6.9 ± 1.6	5.1 ± 0.2
Muscle	1.5 ± 0.4	0.9 ± 0.2	0.8 ± 0.2
Bone	4.3 ± 0.6	5.1 ± 0.5	2.4 ± 0.3
Tumor/Blood	0.8 ± 0.1	1.8 ± 0.3	1.0 ± 0.1
Tumor/Heart	2.3 ± 0.3	5.6 ± 1.4	2.7 ± 0.5
Tumor/Lung	1.2 ± 0.3	3.4 ± 1.2	1.8 ± 0.2
Tumor/Liver	1.3 ± 0.2	2.2 ± 0.4	2.0 ± 0.2
Tumor/Spleen	1.5 ± 0.4	3.4 ± 0.5	3.3 ± 0.8
Tumor/Stomach	7.0 ± 2.8	12.7 ± 2.7	19.4 ± 5.7
Tumor/Sm. Int.	11.5 ± 2.3	20.5 ± 4.8	11.9 ± 1.5
Tumor/Large Int.	5.5 ± 1.1	8.7 ± 4.0	9.7 ± 1.2
Tumor/Kidney	1.5 ± 0.2	3.5 ± 0.9	2.0 ± 0.2
Tumor/Muscle	10.4 ± 3.3	25.4 ± 5.8	13.3 ± 3.1
Tumor/Bone	3.6 ± 0.7	4.7 ± 0.7	4.3 ± 0.6

[a] The data are expressed as the mean %ID/g ± one standard deviation (S.D.). [b] Errors for the Tumor-to-tissue ratios are calculated as the geometric mean of the standard deviations.

Time-activity data from immunoPET imaging

Time-activity data was generated from volume-of-interest (VOI) analysis of the immunoPET imaging of ^{89}Zr-DFO-J591 in male, athymic *nu/nu* mice bearing either s.c. LNCaP (Supplemental Table 9) or PC-3 (Supplemental Table 10) tumors. Standard deviations have been calculated using the data from $n = 3$ animals per tumor group.

Supplemental Table 9. Mean, maximum and median %ID/g TAC data in LNCaP tumors

	LNCaP (n = 3, 60 – 62 μg mAb)			
Time / h	Heart/Blood	Tumor	Liver	Muscle
Mean				
3	15.58 ± 1.25	7.31 ± 1.40	8.39 ± 2.22	1.20 ± 0.26
24	8.14 ± 1.20	18.39 ± 0.87	6.01 ± 1.11	1.35 ± 0.14
48	6.83 ± 0.14	21.89 ± 0.60	5.56 ± 0.56	1.38 ± 0.05
72	4.93 ± 0.86	22.60 ± 0.02	4.62 ± 0.42	1.10 ± 0.12
96	4.27 ± 0.60	20.79 ± 2.23	4.84 ± 0.41	1.11 ± 0.13
120	3.88 ± 0.74	20.33 ± 2.16	4.44 ± 0.10	0.90 ± 0.10
144	3.17 ± 0.42	19.85 ± 0.65	3.14 ± 0.15	0.77 ± 0.12
Maximum				
3	21.44 ± 1.89	11.68 ± 1.38	15.20 ± 3.62	2.58 ± 0.12
24	11.86 ± 0.57	28.90 ± 1.05	10.11 ± 1.32	2.73 ± 0.28
48	9.86 ± 0.23	38.18 ± 4.93	8.00 ± 0.07	2.82 ± 0.11
72	7.68 ± 1.20	49.29 ± 12.88	8.25 ± 0.35	2.73 ± 0.14
96	7.02 ± 0.87	69.14 ± 20.26	7.99 ± 0.39	2.73 ± 0.19
120	7.34 ± 0.83	79.15 ± 26.48	7.52 ± 0.07	2.82 ± 0.38
144	6.78 ± 0.67	92.65 ± 31.27	4.87 ± 0.50	2.59 ± 0.26
Median				
3	15.85 ± 1.34	7.38 ± 1.45	8.32 ± 2.14	1.18 ± 0.28
24	8.39 ± 1.01	19.18 ± 1.00	5.94 ± 1.33	1.35 ± 0.14
48	6.98 ± 0.24	22.55 ± 1.45	5.95 ± 0.51	1.36 ± 0.08
72	5.04 ± 0.87	21.88 ± 2.15	4.95 ± 0.61	1.07 ± 0.13
96	4.29 ±0.63	16.23 ± 1.83	5.00 ± 0.47	1.11 ± 0.13
120	3.87 ± 0.72	14.29 ± 1.45	4.64 ± 0.21	0.89 ± 0.08
144	3.04 ± 0.43	12.74 ± 4.77	3.19 ± 0.16	0.73 ± 0.11
Mean tissue-to-muscle ratio				
3	12.97	6.09	6.99	1.00
24	6.04	13.65	4.46	1.00
48	4.95	15.85	4.03	1.00
72	4.47	20.49	4.19	1.00
96	3.86	18.81	4.38	1.00
120	4.29	22.49	4.91	1.00
144	4.13	25.89	4.10	1.00

Supplemental Table 10. Mean, maximum and median %ID/g TAC data in PC-3 tumors

	PC-3 (n = 3, 60 – 62 μg mAb)			
Time / h	Heart/Blood	Tumor	Liver	Muscle
Mean				
3	15.14 ± 0.36	1.83 ± 0.54	7.88 ± 1.54	0.90 ± 0.00
24	8.17 ± 0.09	4.61 ± 0.40	4.80 ± 0.80	1.26 ± 0.14
48	6.28 ± 0.35	4.84 ± 0.17	5.76 ± 0.06	1.39 ± 0.10
72	5.26 ± 0.32	4.29 ± 0.27	6.12 ± 0.42	1.13 ± 0.06
96	4.99 ± 0.25	4.44 ± 0.12	4.94 ± 0.13	1.20 ± 0.01
120	4.31 ± 0.22	4.44 ± 0.05	5.22 ± 0.46	1.02 ± 0.01
144	3.77 ± 0.03	4.21 ± 0.13	4.93 ± 0.71	1.01 ± 0.17
Maximum				
3	21.19 ± 0.00	3.60 ± 0.44	16.11 ± 4.64	2.42 ± 0.05
24	11.63 ± 0.09	7.81 ± 0.85	11.07 ± 0.05	2.55 ± 0.21
48	9.59 ± 0.38	8.44 ± 0.69	9.73 ± 0.13	3.00 ± 0.10
72	8.60 ± 0.15	8.70 ± 0.01	8.85 ± 0.35	3.01 ± 0.05
96	8.08 ± 0.09	8.00 ± 0.50	8.06 ± 0.15	3.31 ± 0.14
120	6.87 ± 0.19	7.86 ± 0.05	7.55 ± 0.44	2.82 ± 0.01
144	6.31 ± 0.62	7.59 ± 0.01	7.19 ± 0.81	3.19 ± 0.29
Median				
3	15.68 ± 0.17	2.00 ± 0.53	7.92 ± 1.47	0.85 ± 0.05
24	8.61 ± 0.19	4.85 ± 0.37	4.40 ± 1.30	1.28 ± 0.15
48	6.47 ± 0.27	5.15 ± 0.21	6.13 ± 0.03	1.37 ± 0.11
72	5.40 ± 0.38	4.47 ± 0.26	6.38 ± 0.49	1.10 ± 0.05
96	5.10 ± 0.26	4.69 ± 0.06	5.29 ± 0.14	1.15 ± 0.05
120	4.37 ± 0.22	4.62 ± 0.00	5.42 ± 0.43	0.98 ± 0.03
144	3.81 ± 0.01	4.38 ± 0.12	5.14 ± 0.66	0.96 ± 0.14
Mean tissue-to-muscle ratio				
3	16.74	2.02	8.71	1.00
24	6.48	3.66	3.81	1.00
48	4.51	3.48	4.15	1.00
72	4.64	3.79	5.40	1.00
96	4.15	3.70	4.11	1.00
120	4.23	4.36	5.13	1.00
144	3.74	4.19	4.90	1.00

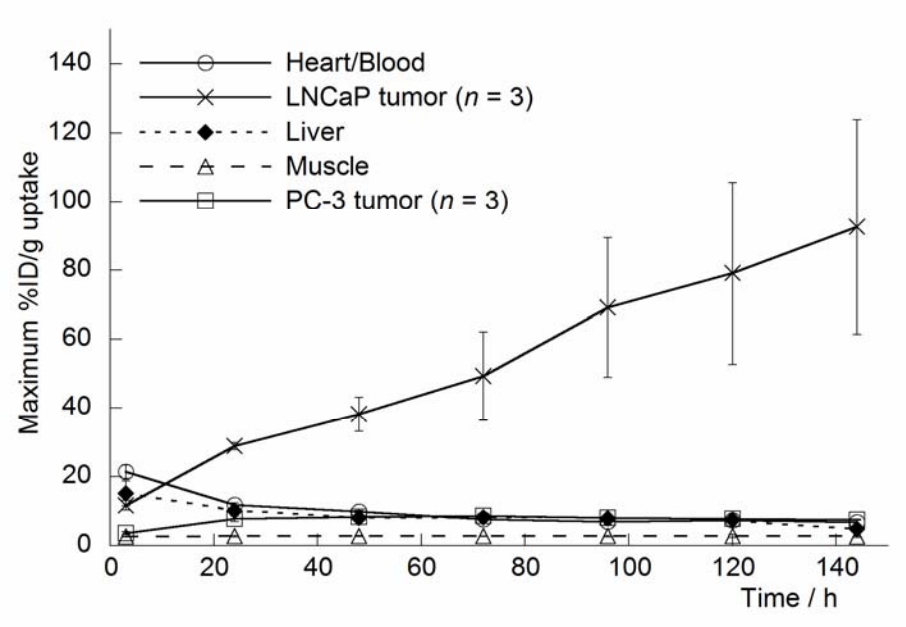

Supplemental Figure 11. Maximum %ID/g TACs for uptake in mice bearing either LNCaP or PC-3 tumors.

NB: Values shown for the maximum %ID/g uptake in the heart/blood, liver and muscle are for mice bearing LNCaP tumors taken from Supplemental Table 9.

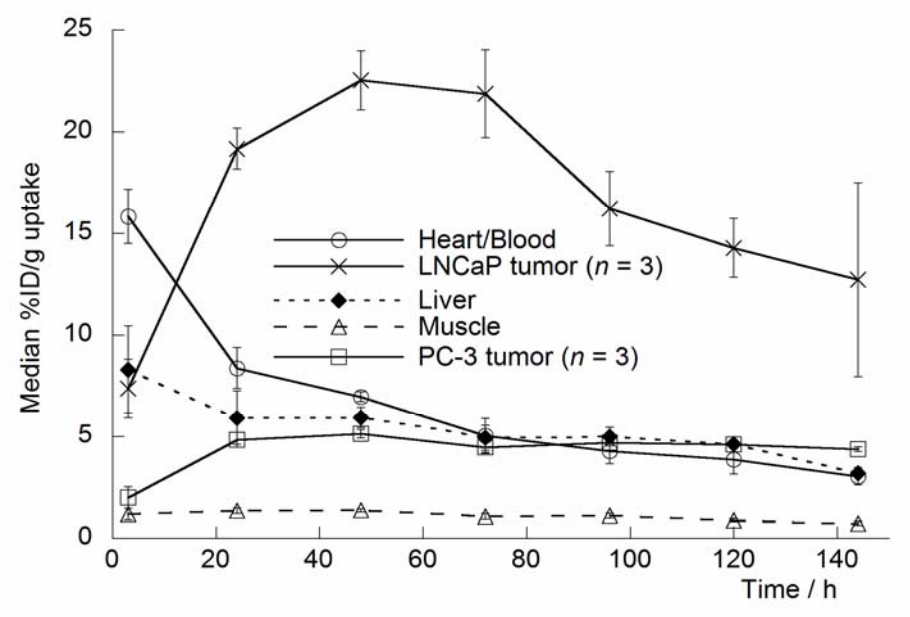

Supplemental Figure 12. Median %ID/g TACs for uptake in mice bearing either LNCaP or PC-3 tumors.

NB: Values shown for the median %ID/g uptake in the heart/blood, liver and muscle are for mice bearing LNCaP tumors taken from Supplemental Table 9.

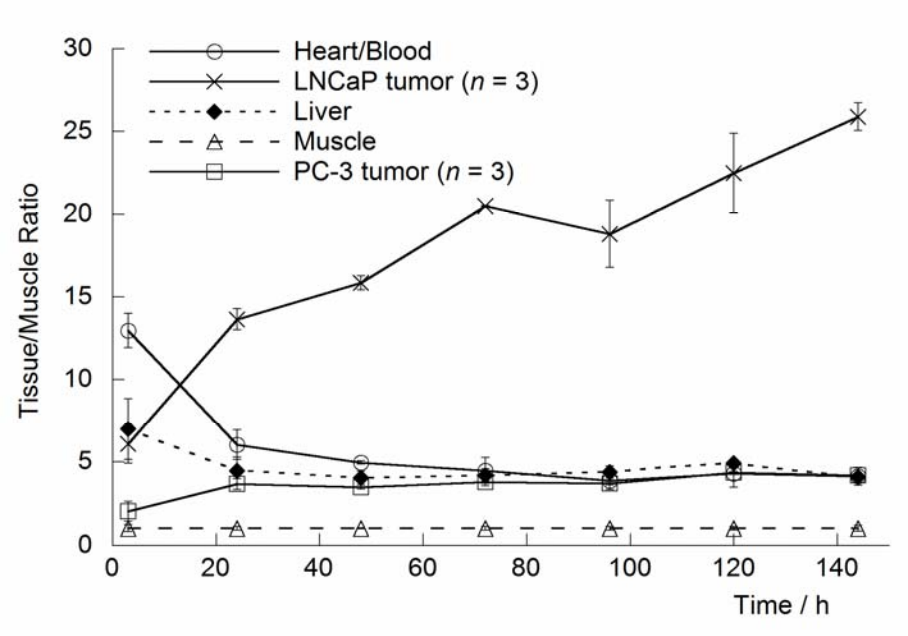

Supplemental Figure 13. Tissue-to-muscle ratio of mean %ID/g uptake TACs in mice bearing either LNCaP or PC-3 tumors.

NB: Values shown for uptake in the heart/blood, liver and muscle are for mice bearing LNCaP tumors taken from Supplemental Table 9.

References

1. Zanzonico P. Routine quality control of clinical nuclear medicine instrumentation: a brief review. *J Nucl Med.* 2009;49(7):1114-1131.

2. Holland JP, Caldas-Lopes E, Divilov V, et al. Measuring the pharmacokinetic effects of a novel Hsp90 inhibitor on HER2/*neu* expression in mice using ^{89}Zr-DFO-trastuzumab. *PLoS ONE.* 2010;5(1):e8859.

3. Kim JS, Lee JS, Im KC, et al. Performance measurement of the microPET Focus 120 scanner. *J Nucl Med.* 2007;48(9):1527-1535.

4. Tseng J-C, Zanzonico PB, Levin B, Finn R, Larson SM, Meruelo D. Tumor-specific in vivo transfection with HSV-1 thymidine kinase gene using a sindbis viral vector as a basis for prodrug ganciclovir activation and PET. *J Nucl Med.* 2006;47:1136-1143.

5. Frisch, M. J.; Trucks, G. W.; Schlegel, H. B.; Scuseria, G. E.; Robb, M. A.; Cheeseman, J. R.; Montgomery, Jr., J. A.; Vreven, T.; Kudin, K. N.; Burant, J. C.; Millam, J. M.; Iyengar, S. S.; Tomasi, J.; Barone, V.; Mennucci, B.; Cossi, M.; Scalmani, G.; Rega, N.; Petersson, G. A.; Nakatsuji, H.; Hada, M.; Ehara, M.; Toyota, K.; Fukuda, R.; Hasegawa, J.; Ishida, M.; Nakajima, T.; Honda, Y.; Kitao, O.; Nakai, H.; Klene, M.; Li, X.; Knox, J. E.; Hratchian, H. P.; Cross, J. B.; Bakken, V.; Adamo, C.; Jaramillo, J.; Gomperts, R.; Stratmann, R. E.; Yazyev, O.; Austin, A. J.; Cammi, R.; Pomelli, C.; Ochterski, J. W.; Ayala, P. Y.; Morokuma, K.; Voth, G. A.; Salvador, P.; Dannenberg, J. J.; Zakrzewski, V. G.; Dapprich, S.; Daniels, A. D.; Strain, M. C.; Farkas, O.; Malick, D. K.; Rabuck, A. D.; Raghavachari, K.; Foresman, J. B.; Ortiz, J. V.; Cui, Q.; Baboul, A. G.; Clifford, S.; Cioslowski, J.; Stefanov, B. B.; Liu, G.; Liashenko, A.; Piskorz, P.; Komaromi, I.; Martin, R. L.; Fox, D. J.; Keith, T.; Al-Laham, M. A.; Peng, C. Y.; Nanayakkara, A.; Challacombe, M.; Gill, P. M. W.; Johnson, B.; Chen, W.; Wong, M. W.; Gonzalez, C.; and Pople, J. A.; Gaussian 03 Revision-C, Gaussian, Inc., Wallingford CT, 2004.

6. Becke AD. Density-functional exchange-energy approximation with correct asymptotic behavior. *Phys Rev A.* 1988;38(6):3098-3100.

7. Lee C, Yang W, Parr RG. Development of the Colle-Salvetti correlation-energy formula into a functional of the electron density. *Phys Rev B.* 1988;37(2):785-789.

8. Rassolov VA, Pople JA, Ratner MA, Windus TL. 6-31G* basis set for atoms K through Zn. *J Chem Phys.* 1998;109(4):1223-1229.

9. Rassolov VA, Ratner MA, Pople JA, Redfern PC, Curtiss LA. 6-31G* basis set for third-row atoms. *J Comput Chem.* 2001;22(9):976-984.

10. Holland JP, Sheh Y, Lewis JS. Standardized methods for the production of high specific-activity zirconium-89 *Nucl Med Biol.* 2009;36(7):729-739.

11. Verel I, Visser GWM, Boellaard R, Stigter-van Walsum M, Snow GB, van Dongen GAMS. ^{89}Zr immuno-PET: Comprehensive Procedures for the production of ^{89}Zr-labeled monoclonal antibodies. *J Nucl Med.* 2003;44:1271-1281.

12. Anderson CJ, Schwarz SW, Connett JM, et al. Preparation, biodistribution and dosimetry of copper-64-labeled anti-colorectal carcinoma monoclonal antibody fragments 1A3-F(ab')$_2$. *J Nucl Med.* 1995;36(5):850-858.

13. Lindmo T, Boven E, Cuttitta F, Fedorko J, Bunn PA, Jr. Determination of the immunoreactive fraction of radiolabeled monoclonal antibodies by linear extrapolation to binding at infinite antigen excess. *J Immunol Methods.* 1984;72(1):77-89.